Momentum transfer in complex plasmas

Sergey A. Khrapak,* Alexey V. Ivlev, and Gregor E. Morfill
Centre for Interdisciplinary Plasma Science, Max-Planck-Institut für Extraterrestrische Physik, D-85741 Garching, Germany
(Received 14 June 2004; published 16 November 2004)

Momentum transfer in complex plasmas (systems consisting of ions, electrons, neutrals, and charged macroscopic grains) is investigated assuming an interaction potential between the charged species of the screened Coulomb (Yukawa) type. Momentum transfer cross sections and rates are derived. Applications of the results are discussed; in particular, we classify the possible states of complex plasmas in terms of the momentum transfer due to grain-grain collisions and its competition with that due to interaction with the surrounding medium. The resulting phase diagrams are presented.

DOI: 10.1103/PhysRevE.70.056405 PACS number(s): 52.27.Lw, 52.20.Hv, 52.20.−j

I. INTRODUCTION

Complex plasmas consist of ions, electrons, highly charged micron-sized particles (dust grains), and neutral gas. Depending on the strength of the interaction (coupling) between the grains (which can be easily varied experimentally over a fairly wide range), complex plasmas can exhibit properties of crystals, liquids, and gases. In addition, the overall dynamical time scales associated with the grain component are relatively long and the grains can be easily visualized. The unique feature of observing kinetic properties in real space and time provides the opportunity to study generic universal processes (e.g., phase transitions, crystallization, relaxation to the final equilibrium state, self-organization and scaling in fluid flows, transition from "matter" to particles, etc.) in a detail not possible so far, and at a more fundamental level. For the current state of the field, see the recent review papers [1–9].

The momentum exchange between different species plays an exceptionally important role in complex plasmas. For example, the momentum transfer in collisions with the neutral gas "cool down" the system, in particular grains and ions, introducing some damping. The forces associated with the momentum transfer from electrons and ions to the charged grains—i.e., the electron and ion drag forces—often determine static and dynamical properties of the grain component, affect wave phenomena, etc. The momentum transfer in grain-grain collisions and its competition with the momentum transfer in grain-neutral gas collisions governs grain transport properties, scalings in fluid flows, etc. While various aspects of electron-ion interaction (collisions) as well as electron, ion, and grain collisions with neutrals have been well studied, comparatively little work has been done on grain-electron, grain-ion, and grain-grain collisions.

In this paper, we report on a detailed analysis of the collisions involving dust grains. Assuming a screened Coulomb (Debye-Hückel or Yukawa) interaction potential (attractive or repulsive), the momentum-transfer cross sections for pair collisions of particles are calculated. We show that for typical complex plasma parameters, the theory of Coulomb scattering is applicable only for electron-grain collisions, while for ion-grain and grain-grain collisions, different approaches should be used. Based on numerical calculations, the required approaches are developed, the role of finite grain size is investigated, and analytical approximations for the momentum-transfer cross sections are proposed. The latter are used to estimate the characteristic momentum-transfer rates in complex plasmas. This provides us with a unified theory of momentum transfer in complex plasmas in the pair collision approximation.

Some direct applications of the results are considered. First, we briefly discuss calculations of the electron and ion drag forces. Then we develop criteria to classify the possible states of complex plasmas in terms of the momentum transfer. In particular, we identify the conditions for different states: ideal and nonideal plasma, as well as two different types of granular medium. Finally, we investigate the hierarchy of the momentum transfer in grain-grain and grain-neutral collisions and show that complex plasmas can exist in a broad range of dynamical states: one- and two-phase fluids and tracer particles. The obtained results can be important for "engineering" experiments which aim to make use of special properties of complex plasmas.

II. MOMENTUM-TRANSFER CROSS SECTION

A. Approach

We consider pair interactions and assume ballistic trajectories of particles during collisions (i.e., we neglect any type of multiple collisions). We assume a Yukawa potential for the interaction between charged particles in complex plasmas,

$$U(r) = -(U_0/r)\exp(-r/\lambda), \tag{1}$$

where $U_0 > 0$ for attraction and $U_0 < 0$ for repulsion. We also use Maxwellian velocity distribution functions for all species. These assumptions allow us to simplify the calculations, but we should bear in mind that not all of them are necessarily satisfied in reality. A few examples are as follows: deviation of grain potential from the Yukawa form [1,6,8,10], dependence of the grain charge on intergrain distance [8], destruction of ballistic trajectories by collisions with neutrals [11], etc. Nevertheless, in many cases this simple model does

*Electronic address: skhrapak@mpe.mpg.de

provide reasonable predictions and hence it can be considered as the basis for more sophisticated models.

We consider a collision between two particles of masses m_1 and m_2 interacting via an isotropic potential of the form of Eq. (1). This problem is equivalent to the scattering of a single particle of reduced mass, $\mu=m_1m_2/(m_1+m_2)$, in a field $U(r)$ (whose center is at the center of masses of the colliding particles). First, we study the case of pointlike particles. The role of the finite grain size will be addressed later. The momentum-transfer (scattering) cross section is given by (see, e.g., [12])

$$\sigma_s = 2\pi \int_0^\infty [1-\cos\chi(\rho)]\rho d\rho, \tag{2}$$

where ρ is the impact parameter and χ is the deflection (scattering) angle. The latter depends on the impact parameter in the following way, $\chi(\rho)=|\pi-2\varphi(\rho)|$, where $\varphi(\rho)=\rho\int_{r_0}^\infty dr r^{-2}[1-U_{\rm eff}(r,\rho)]^{-1/2}$ and $U_{\rm eff}(r,\rho)=\rho^2/r^2+U(r)/\varepsilon$ is the effective potential energy (normalized by the kinetic energy $\varepsilon=\mu v^2/2$). The distance of closest approach, $r_0(\rho)$, in the integral above is the largest root of the equation

$$U_{\rm eff}(r,\rho)=1. \tag{3}$$

Using these expressions, σ_s can be calculated for arbitrary potential $U(r)$.

B. Scattering parameter

For the Yukawa interaction potential, the following important dimensionless parameter can be introduced [13–16]:

$$\beta(v)=|U_0|/\mu v^2\lambda, \tag{4}$$

which is the ratio of the Coulomb radius, $R_C=|U_0|/\mu v^2$, to the screening length λ. It characterizes the "scattering range": The scattering is "short range" when the characteristic distance of interaction $R_0\sim R_C$, introduced through $|U(R_0)|=\varepsilon$, is shorter than the screening length, i.e., when $\beta(v)\ll 1$. In the opposite limit, $\beta(v)\gg 1$, when $R_0\gg\lambda$, the scattering is called "long range." Also the normalized momentum-transfer (scattering) cross section, σ_s/λ^2, depends only on β [15–17]. Hence, $\beta(v)$ is a *unique parameter* which describes momentum transfer for Yukawa interactions.

Note that the theory of Coulomb scattering, which assumes an unscreened Coulomb potential and a cutoff at $\rho_{\max}=\lambda$ in the integral (2), is widely used to describe momentum transfer in collisions between charged particles (e.g., electron-ion collisions in plasmas). It holds for $R_C\sim R_0\ll\lambda$ or $\beta\ll 1$, i.e., in the limit of short-range scattering. However, for $\beta\gtrsim 1$, the theory of Coulomb scattering is not applicable: In this case, the scattering range R_0 is larger than the screening length and a considerable fraction of the interaction occurs outside the Debye sphere providing substantial contribution to the momentum transfer. The use of a cutoff at $\rho_{\max}=\lambda$ considerably underestimates the momentum transfer in this case [13–16].

Now let us estimate the characteristic values of the scattering parameter for different types of collisions involving dust grains. Taking into account that $|U_0|\sim|Z|e^2$ for grain-electron and grain-ion collisions, and $|U_0|\sim Z^2e^2$ for grain-grain collisions, we get the following hierarchy of characteristic scattering parameters: (i) *Electron-grain* collisions, $\beta_T^{ed}\sim z(a/\lambda)\sim 0.01$–$0.3$; (ii) *ion-grain* collisions, $\beta_T^{id}\sim z\tau(a/\lambda)\sim 1$–$30$; *grain-grain* collisions, $\beta_T^{dd}\sim z_d(a/\lambda)\sim 10^3$–$3\times10^4$. Here the subscript "$T$" stands for the thermal velocity, $v_T=\sqrt{T/m}$, with T and m the temperature and the mass of the lightest species, and Z and a are the grain charge number and grain radius, respectively. We have used the following dimensionless parameters: $z=|Z|e^2/aT_e$, grain surface potential in units of electron temperature; $z_d=Z^2e^2/aT_d\equiv z|Z|(T_e/T_d)$, normalized potential energy of two dust grains which are just touching; and $\tau=T_e/T_i$, electron-to-ion temperature ratio. We also assumed $z\sim 1$, $\tau\sim 10^2$, $a/\lambda\sim 0.01$–0.3, $|Z|\sim 10^3$, and $z_d=z|Z|\tau=10^5$ (for $T_d=T_i$), which is typical for complex plasmas.

These estimates show that the scattering is typically short range only for electron-grain collisions. At the same time, scattering in ion-grain and grain-grain collisions is long range, and the theory of Coulomb scattering fails to describe such collisions. In connection with ion-grain collisions, this issue was recently discussed in detail in Refs. [13–16].

C. Calculations for pointlike particles

We calculated numerically the momentum-transfer cross sections for β in the range from 0.1 to 10^3, both for attractive and repulsive Yukawa potential. First, the dependence of the scattering angle on the impact parameter, $\chi(\rho)$, was obtained. Then, Eq. (2) was numerically integrated yielding the momentum-transfer cross sections. The results are presented in Figs. 1 and 2.

The scattering angle $\chi(\rho)$ decreases monotonically for repulsive interactions for all β. In contrast, for attractive interactions a monotonous decrease of the scattering angle is observed only for $\beta\lesssim 1$, while for $1\lesssim\beta\lesssim\beta_{\rm cr}$ it becomes a nonmonotonous function of ρ, and at $\beta>\beta_{\rm cr}\simeq 13.2$ the scattering angle diverges at "transitional" impact parameter $\rho_*\simeq\lambda\left(\ln\beta+1-\frac{1}{2}\ln^{-1}\beta\right)$. The divergence of the scattering angle for attractive interactions arises from the barrier in the effective potential energy $U_{\rm eff}$, which emerges at $\beta>\beta_{\rm cr}$. Note also that when $\beta\ll 1$, the trajectories are mainly deflected within the Debye radius (at $\rho/\lambda\lesssim 1$). In the opposite case $\beta\gg 1$, the scattering angle can be substantial even for $\rho>\lambda$, both for repulsive and attractive interaction. (This is another demonstration of the fact that the Coulomb scattering theory is inapplicable for $\beta\gtrsim 1$, as discussed above.)

The results obtained for the momentum-transfer cross section (Fig. 2) show the following features: The cross section for the attractive potential is always larger than that for the repulsive potential (they converge in the limit of short-range scattering $\beta\ll 1$). The cross section for the repulsive potential grows monotonically, while for the attractive potential a local maximum and minimum appear near $\beta=\beta_{\rm cr}$. This nonmonotonic behavior is a consequence of the bifurcation which the scattering angle $\chi(\rho)$ experiences in the range $1\lesssim\beta\lesssim\beta_{\rm cr}$. It is also clear from Fig. 2 that the Coulomb scattering theory (shown by the dotted line) considerably under-

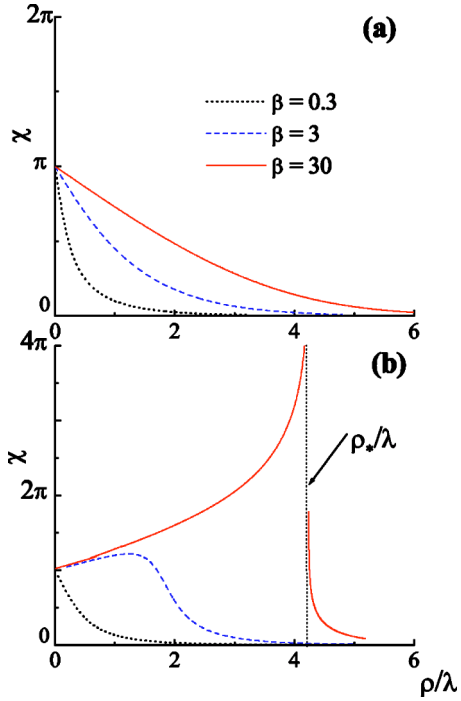

FIG. 1. (Color online) Scattering angle χ vs the normalized impact parameter ρ/λ, where λ is the screening length. The numerical calculations for a repulsive (a) and attractive (b) Yukawa interaction potential are plotted for three different scattering parameters β=0.3, 3, and 30. The vertical dotted line at $\rho \simeq 4.2\lambda$ in (b) indicates the transitional impact parameter ρ_* at which χ diverges.

estimates the cross section for both repulsion and attraction when $\beta \gtrsim 1$.

Now we consider different limiting cases when an analytical description for the momentum-transfer cross section is possible.

Repulsive potential. In the limit of short-range scattering, the Coulomb scattering theory is applicable as discussed above. The well known expression for the *Coulomb* scattering cross section

$$\sigma_s^C/\pi\lambda^2 = 2\beta^2 \ln(1 + 1/\beta^2) \tag{5}$$

is shown by the dotted line in Fig. 2. For $\beta \gtrsim 1$, Eq. (5) is no longer applicable, however an asymptotic analytical approximation for the case $\beta \gg 1$ can be obtained as follows: The parameter β characterizes the "steepness' of the Yukawa potential. The relevant characteristic of the steepness is the parameter $\gamma_0 = |d \ln U(r)/d \ln r|_{r=R_0}$, which is roughly the ratio of the interaction radius R_0 to the depth of the interaction "shell." Depending on a value of γ_0, the potential can be called "hard" ($\gamma_0 \gg 1$) or "soft" ($\gamma_0 \ll 1$). Physically, the case $\gamma_0 \gg 1$ corresponds to a rapidly decreasing potential $U(r)$, so that the momentum is mostly transferred in a spherical "shell" of radius R_0 and thickness $\sim R_0/\gamma_0$. Hence, the scattering resembles that of a hard-sphere potential [18]. For an arbitrary potential, the expansion of the *hard-sphere* momentum-transfer cross section over the small parameter γ_0^{-1} yields [19]

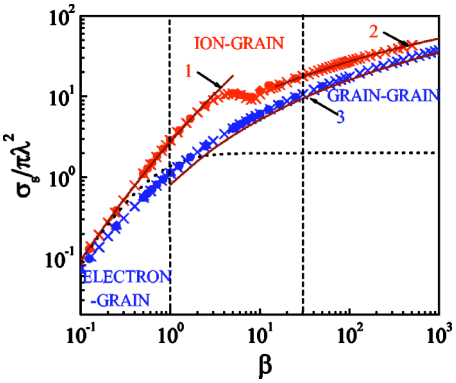

FIG. 2. (Color online) Momentum-transfer cross section, σ_s, normalized to $\pi\lambda^2$ (where λ is the screening length), vs the scattering parameter β. The upper data are for attractive and the bottom data are for repulsive screened Coulomb potentials. Crosses correspond to our numerical calculation, circles are numerical results by Hahn *et al.* [20], and triangles are numerical results by Lane and Everhart [17]. Solid curves correspond to the following analytical expressions: 1, Eq. (8); 2, Eq. (9); 3, Eq. (6). The dotted line corresponds to the Coulomb scattering theory [Eq. (5)]. All the results are for pointlike particles. Vertical dashed lines conditionally divide the β axis into three regions: $\beta \ll 1$ is typical of electron-grain collisions; $1 \lesssim \beta \lesssim 30$ is typical of ion-grain collisions; $\beta \gg 1$ is typical of grain-grain collisions. For details, see text.

$$\sigma_s^{HS}/\pi\lambda^2 \simeq (R_0/\lambda)^2[1 + \gamma_0^{-1}(3 - 4\ln 2) + O(\gamma_0^{-2})]. \tag{6}$$

For the Yukawa potential, $\gamma_0 = 1 + R_0/\lambda$. Figure 3 shows the dependence of the interaction radius R_0 on β [obtained from Eq. (3) for $\rho = 0$]. One can see that $R_0 \gg \lambda$ for $\beta \gg 1$ and hence $\gamma_0 \gg 1$. We note that for the Yukawa interaction potential, a rapidly converging analytical solution for $R_0(\beta)$ can be obtained. Keeping only the first two terms of the expansion, we get

$$R_0/\lambda \simeq \ln 2\beta - \ln\ln 2\beta. \tag{7}$$

For very large β, the first term is dominant so that $R_0 \simeq \lambda \ln 2\beta$.

Attractive potential. For short-range scattering ($\beta \ll 1$),

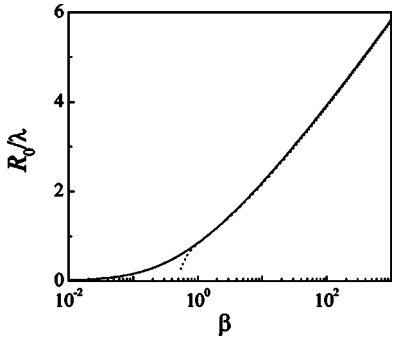

FIG. 3. The normalized interaction radius R_0/λ, where λ is the screening length, vs the scattering parameter β for the screened Coulomb potential. The solid line corresponds to the exact solution of Eq. (3) with $\rho = 0$, the dashed line shows an approximate solution given by Eq. (7).

the theory of Coulomb scattering is applicable. The momentum-transfer cross section is the same as for the repulsive potential and is given by Eq. (5). It was shown recently by Khrapak *et al.* [13,14] that even for moderate β the extension of the standard Coulomb scattering theory is possible by taking into account collisions with impact parameters above λ. In Refs. [13,14], the maximum impact parameter is determined by taking all the trajectories with a distance of closest approach shorter than λ into account. The definition of the maximum impact parameter (cutoff) then becomes $r_0(\rho_{\max})=\lambda$ instead of $\rho_{\max}=\lambda$ (note that both definitions are equivalent in the limit $\beta \ll 1$). This leads to a modification of the Coulomb logarithm. The *modified Coulomb* momentum-transfer cross section can be written as

$$\sigma_s^{\mathrm{MC}}/\pi\lambda^2 \simeq 4\beta^2 \ln(1+1/\beta). \tag{8}$$

Although the approach of [13,14] is not rigorous, Eq. (8) shows very good agreement with numerical results [20,21] up to $\beta \sim 5$ (see Fig. 2) and agrees exactly, of course, with Coulomb scattering theory for $\beta \ll 1$.

The case of long-range scattering ($\beta \gg 1$) requires a new physical approach. Such an approach was formulated in Ref. [15]. The existence of the potential barrier in U_{eff} at $\beta > \beta_{\mathrm{cr}}$ and the discontinuity in $\chi(\rho)$ it causes play a crucial role for the analysis of collisions. As shown in Fig. 1, the dependence of the scattering angle on the impact parameter in the limit of long-range scattering ($\beta=30$) has the following features: For "close" ($\rho < \rho_*$) collisions we have $\chi \to \pi$ at $\rho \to 0$, and $\chi(\rho)$ grows monotonically until $\rho=\rho_*$, where it diverges; for "distant" collisions ($\rho > \rho_*$), the scattering angle decreases rapidly, due to the exponential screening of the interaction potential.

It is convenient to consider the contributions from close and distant collisions into the momentum transfer separately. As shown in Ref. [15], the behavior of χ as a function of the normalized impact parameter ρ/ρ_* is *practically independent* of β for $\rho < \rho_*$. This self-similarity allows us to present this contribution to the cross section (normalized to $\pi\lambda^2$) as $\simeq \mathcal{A}(\rho_*/\lambda)^2$, where $\mathcal{A}=2\int_0^1[1-\cos\chi(\xi)]\xi d\xi$ and $\xi=\rho/\rho_*$. The numerical factor $\mathcal{A}$ can be determined by direct numerical integration. It was found that $\mathcal{A}=0.81\pm0.01$ for all β in the range $\beta_{\mathrm{cr}} \leqslant \beta \leqslant 500$ [15]. For distant collisions, the scattering angle decreases rapidly in the vicinity of ρ_*. This makes it possible to apply the small-angle approximation to estimate their contribution to the cross section (normalized to $\pi\lambda^2$) as $\simeq 2.0+4.0\ln^{-1}\beta$ [15]. Combining these contributions and keeping terms up to $O(1)$, we can write the momentum-transfer cross section in the limit of *long-range* scattering as

$$\sigma_s^{\mathrm{LR}}/\pi\lambda^2 \simeq 0.81(\rho_*/\lambda)^2 + 2.0, \tag{9}$$

where $(\rho_*/\lambda)^2 \simeq \ln^2\beta + 2\ln\beta$. Expression (9) is valid for $\beta \geqslant \beta_{\mathrm{cr}}$ and pointlike particles. Figure 2 shows the very good agreement between Eq. (9) and numerical calculations. A sufficiently accurate and even simpler approximation is $\sigma_s^{\mathrm{LR}} \simeq \pi\rho_*^2$, which will be further justified in the next section where the finite size of the dust grain is taken into account.

D. Role of finite particle size

We consider the collision of two (spherical) particles interacting via a Yukawa potential and having *finite radii* (b_1 and b_2). The problem is equivalent to the scattering of a pointlike particle at the center of radius $b=b_1+b_2$, i.e., a new length scale enters the problem. In contrast to the case of pointlike particles, where the scattering is described by the single parameter β, we now have a second parameter, b/λ. If the distance of the closest approach, r_0, is smaller than b, then the direct (touching) collision takes place.

For the repulsive interaction (electron-grain and grain-grain collisions), the orbital motion limited (OML) approach [22,23] is always applicable and yields for the maximum impact parameter corresponding to touching collisions (assuming $b \ll \lambda$)

$$\rho_c \simeq b\sqrt{1-2\beta(\lambda/b)}.$$

The momentum-transfer cross section in touching collisions (assuming absorption for electrons and specular reflection for the grains) is $\sigma_c=\pi\rho_c^2$, so that

$$\sigma_c \simeq \begin{cases} \pi b^2[1-2\beta(\lambda/b)], & \beta < b/2\lambda \\ 0, & \beta \geqslant b/2\lambda. \end{cases} \tag{10}$$

Obviously, we get $b=a$ for electron-grain collisions and $b=2a$ for grain-grain collisions. For $\beta \lesssim a/\lambda \ll 1$, the Coulomb scattering theory can be used to estimate the contribution from scattering. Comparing Eqs. (5) and (10) we get an approximate condition when the momentum transfer in touching collisions dominates over that due to the Coulomb scattering. For both types of collisions, this condition is

$$\beta \lesssim (a/\lambda)\Lambda^{-1/2}, \tag{11}$$

where $\Lambda \simeq \ln(1/\beta) \gg 1$ is the Coulomb logarithm. Recalling that $\beta_T^{ed} \sim z(a/\lambda)$ and $\beta_T^{dd} \sim z_d(a/\lambda)$ and since $z \sim 1$, the effect of finite size can usually be neglected for electron-grain collisions. For grain-grain collisions, it is substantial provided $z_d=z|Z|(T_e/T_d) \ll 1$, i.e., for extremely high grain temperatures $T_d \gg |Z|T_e$.

The effect of finite size is more important for attractive (ion-grain) interactions. As in previous consideration, ion collection occurs if the impact parameter is smaller than ρ_c. If $\rho_c < \rho_*$, then Eq. (3) has a single root and the OML theory can be applied yielding for attraction ($b=a$ for ion-grain collisions)

$$\rho_c = a\sqrt{1+2\beta(\lambda/a)} \equiv \rho_c^{\mathrm{OML}}. \tag{12}$$

At very large β, however, $\rho_c^{\mathrm{OML}} \propto \sqrt{\beta}$ exceeds the transitional impact parameter, $\rho_* \propto \lambda\ln\beta$. That means that the OML approach is no longer applicable, because for particles having $\rho \geqslant \rho_*$, Eq. (3) has multiple roots. These particles experience distant collisions, with r_0 considerably larger than λ, and therefore are not absorbed. Thus the absorption radius for very large β equals the transitional impact parameter: $\rho_c=\rho_*$.

The total momentum-transfer cross section for finite-size particles consists generally of collection and scattering parts: $\sigma_\Sigma=\sigma_c+\tilde{\sigma}_s$. The collection momentum-transfer cross section is $\sigma_c=\pi\rho_c^2$. The scattering part $\tilde{\sigma}_s$ is given by Eq. (2), with

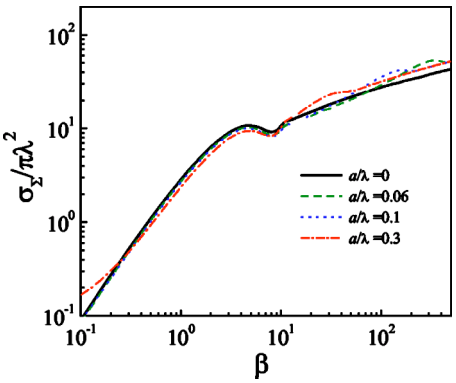

FIG. 4. (Color online) The total momentum-transfer cross section, σ_Σ, normalized to $\pi\lambda^2$ (where λ is the screening length), vs the scattering parameter β for the attractive screened Coulomb potential. The numerical results for different values of a/λ are shown to illustrate the role of finite particle radius a.

the lower limit of integration replaced by ρ_c. For a repulsive potential collection is unimportant and $\sigma_\Sigma \sim \tilde{\sigma}_s \sim \sigma_s$. The dependence $\sigma_\Sigma(\beta)$ for an attractive potential is shown in Fig. 4 for different values of a/λ. One can see from Fig. 4 that the momentum transfer can decrease or increase (in comparison with pointlike particles), depending on the values of a/λ and β. For sufficiently large β (when $\rho_c = \rho_*$), the total cross section is $\sigma_\Sigma/\pi\lambda^2 \simeq (\rho_*/\lambda)^2 + 2.0$. As $\beta \to \infty$, the relative contribution of distant collisions vanishes and σ_Σ tends to $\pi\rho_*^2$, the collection cross section. At the same time, the momentum-transfer cross section is not very sensitive to the particle size—the deviation of σ_Σ from σ_s does not exceed $\sim 50\%$. Hence for practical purposes the total momentum-transfer cross section, σ_Σ, can be approximated quite well by the scattering cross section for pointlike particles [Eq. (8) for $\beta \lesssim 5$], or by $\pi\rho_*^2$ in the limit $\beta \gg \beta_{cr} \simeq 13.2$ [15,16].

Concluding this section, we would like to comment on the applicability of the OML approach to calculate the ion collection by grains. As we found above, OML is applicable when $\rho_c^{OML} \leqslant \rho_*$. For a Maxwellian ion velocity distribution there are *always* sufficiently slow ions, for which this condition is violated [24]. However, if this inequality is satisfied for most of the ions, corrections to OML are small. This requires ρ_c^{OML} to be considerably smaller than ρ_* for $\beta = \beta_T^{id}$. Using our dimensionless parameters, we can rewrite this condition in the form

$$\sqrt{2z\tau}(a/\lambda) \lesssim \ln[z\tau(a/\lambda)]. \tag{13}$$

[Note that we consider the case when $\beta_T^{id} \equiv z\tau(a/\lambda) \geqslant 13.2$.] It applies when the self-consistent potential distribution around the grain is well represented by a screened Coulomb form [6,23]. For typical complex plasma parameters $z \sim 1$ and $\tau \sim 100$, we get that OML is applicable for $a/\lambda \lesssim 0.2$, i.e., for most cases of interest. When OML fails, it overestimates the ion flow on the grain and hence underestimates the floating potential. Note that the ion-neutral collisions, which are neglected in our consideration, can also affect the grain charging. The collisions "eliminate" the ion angular momentum, which enhances the ion current, and, thus suppress the floating potential [23,25–27].

III. MOMENTUM-TRANSFER RATES

Momentum-transfer rates can be derived as follows: Let us consider a *test* particle (dust grain) moving with a velocity $\mathbf{u}_t$ through a gas of *field* particles (electrons, ions, or dust grains) having an isotropic velocity distribution function f_f. On average, collisions with the field particles do not change the direction of $\mathbf{u}_t$, but cause its absolute value to decrease. The equation of motion for the test particle is

$$m_d \frac{du_t}{dt} = N\mu \int v \cos\theta \sigma(v) v f_f(|\mathbf{v} + \mathbf{u}_t|) d\mathbf{v}, \tag{14}$$

where m_d is the mass of the dust grain, N is the number density of field particles, σ is the momentum-transfer cross section, which is a function of the relative velocity $v = |\mathbf{u}_f - \mathbf{u}_t|$, and θ is the angle between vectors $\mathbf{u}_t$ and $\mathbf{v}$. Assuming a Maxwellian velocity distribution function for the field particles and slow motion of the test particle (i.e., $u_t \ll u_{T_f}$, where u_{T_f} denotes thermal velocity of the field particles), we get $f_f(|\mathbf{v} + \mathbf{u}_t|) \simeq f_f(v)[1 - (v u_t / u_{T_f}^2)\cos\theta]$. The symmetric component of the distribution $f_f(v)$ does not contribute to the resistance force. Introducing the momentum transfer rate ν through $du_t/dt = -\nu u_t$, we get after integration over the angles

$$\nu = \frac{1}{3}\sqrt{\frac{2}{\pi}} \frac{N\mu}{m_d u_{T_f}^5} \int_0^\infty v^5 \sigma(v) \exp(-v^2/2u_{T_f}^2) dv. \tag{15}$$

Some special applications of this expression are given below.

A. Electron-grain collisions

For electron-grain interactions usually $\beta_T^{ed} \ll 1$ and the standard Coulomb scattering approach is applicable. This yields

$$\nu_{ed} \simeq (2\sqrt{2\pi}/3)(m_e/m_d) n_e v_{T_e} a^2 z^2 \Lambda_{ed}, \tag{16}$$

where n_e, m_e, and v_{T_e} are the density, mass, and thermal velocity of electrons, and

$$\Lambda_{ed} = z \int_0^\infty e^{-zx} \ln[1 + 4(\lambda/a)^2 x^2] dx - 2z \int_1^\infty e^{-zx} \ln(2x - 1) dx \tag{17}$$

is the Coulomb logarithm for electron-grain collisions integrated over the Maxwellian distribution [28]. In the typical case $(2/z)(\lambda/a) \gg 1$, we obtain $\Lambda_{ed} \simeq 2\ln[(2/z)(\lambda/a)]$ with logarithmic accuracy. This result is an improvement of the Coulomb logarithm $\Lambda_{ed} \sim 2\ln(\lambda/a)$ used in the literature (see, e.g., [29]). The derived momentum transfer rate can be employed to estimate the electron drag force in the subthermal regime for electron drift, $F_e = m_d \nu_{ed} u_e$, where u_e denotes the electron drift velocity. Detailed investigation of the role of the electron drag force under different plasma conditions can be found in Ref. [28].

B. Ion-grain collisions

For ion-grain interaction β_T^{id} often exceeds unity and then the Coulomb scattering approach is not applicable. In the case $\beta_T^{id} \lesssim 5$, Eq. (8) can be used. This yields

$$\nu_{id} \simeq (2\sqrt{2\pi}/3)(m_i/m_d) n_i v_{T_i} a^2 z^2 \tau^2 \Lambda_{id}, \tag{18}$$

where n_i, m_i, and v_{T_i} are the density, mass, and thermal velocity of ions, and

$$\Lambda_{id} \simeq 2z \int_0^\infty e^{-zx} \ln[1 + 2\tau^{-1}(\lambda/a)x] dx \tag{19}$$

is the *modified* Coulomb logarithm for ion-grain scattering [13,14] integrated over the Maxwellian distribution [in Eq. (19) we took into account that $\tau \gg 1$]. In the limit of small β_T^{id} or $(1/z\tau)(\lambda/a) \gg 1$, the result reduces to that of the Coulomb scattering theory. We have then $\Lambda_{id} \simeq 2 \ln[(2/z\tau)(\lambda/a)]$, which is considerably smaller than the value $\ln(\lambda/a)$ used previously [29]. In the opposite limit of very large scattering parameters, $\beta_T^{id} > \beta_{cr} \simeq 13.2$, the total momentum-transfer cross section can be taken as $\sigma_\Sigma \simeq \pi \rho_*^2$, with a good accuracy as shown above, where $\rho_* \sim \lambda \ln \beta_T^{id}$. This yields

$$\nu_{id} \simeq (8\sqrt{2\pi}/3)(m_i/m_d) n_i v_{T_i} \rho_*^2. \tag{20}$$

The momentum-transfer rates [Eqs. (18)–(20)] were recently used to estimate the ion drag force, $F_i = m_d \nu_{id} u_i$, in complex plasmas with subthermal ($u_i \lesssim v_{T_i}$ ion drifts). The details can be found in Refs. [13–16].

C. Grain-grain collisions

For grain-grain interactions, the standard Coulomb scattering approach can be employed only for extremely small grain charges and/or extremely high grain energies, so that $\beta_T^{dd} = z_d(a/\lambda) \ll 1$. In this situation, we have

$$\nu_{dd} \simeq (4\sqrt{2\pi}/3) n_d v_{T_d} a^2 z_d^2 \Lambda_{dd}, \tag{21}$$

where n_d and v_{T_d} are the density, and thermal velocity of the dust grains, and

$$\Lambda_{dd} = z_d \int_0^\infty e^{-z_d x} \ln[1 + (\lambda/a)^2 x^2] dx - 2z_d \int_1^\infty e^{-z_d x} \ln(2x - 1) dx \tag{22}$$

is the Coulomb logarithm for grain-grain collisions integrated over the Maxwellian distribution. The form of this expression is similar to that of Eq. (17). If $(1/z_d)(\lambda/a) \gg 1$, the Coulomb scattering approach is applicable and we have $\Lambda_{dd} \simeq 2 \ln[(1/z_d)(\lambda/a)]$ with logarithmic accuracy. However, the limit of long-range scattering, $\beta_T^{dd} \gg 1$, is more typical for complex plasmas and then the analogy with hard-sphere collisions can be used. According to Eq. (6), the momentum transfer cross section $\sigma_s^{HS} \simeq \pi R_0^2 [1 + 0.23/(1 + R_0/\lambda)]$, with R_0 taken from Eq. (7). Since R_0/λ considerably exceeds unity, we can approximately write

$$\nu_{dd} \simeq (4\sqrt{2\pi}/3) n_d v_{T_d} R_0^2. \tag{23}$$

Equations (21)–(23) will be used in the next section to investigate the possible states of complex plasmas.

IV. PHASE DIAGRAM OF COMPLEX PLASMAS

The grain charges in complex plasmas, as well as the plasma screening length, are not constant. This is why the strength of the electrostatic coupling between the grains can be easily changed experimentally over a fairly wide range (by varying, e.g., the discharge conditions [30]). This is a major distinguishing feature of complex plasmas compared to usual plasmas, where the ion charges are normally constant (single). The latter implies low coupling strength in usual plasmas (although one can, in principle, obtain fairly strong coupling in non-neutral plasmas, e.g., ionic crystals [31]). In complex plasmas, one can observe the transitions from the disordered, weakly coupled to strongly coupled states and the formation of ordered structures of grains—plasma crystals [1–9,32–36].

Another major distinguishing feature of complex plasmas is that the overall dynamical time scales associated with the dust component are relatively long (dust plasma frequency $\sim 10-100$ Hz) [1,3,37]. Furthermore, the grains themselves are large enough to be easily visualized individually. All together this makes it possible to investigate phenomena occurring in different phases at the most fundamental kinetic level [5,6,30]. Although there is always some damping introduced into the complex plasma systems due to neutral gas friction [3], the resulting damping rate is many orders of magnitude smaller than that in colloidal suspensions, and it can easily be made much smaller than the major eigenfrequencies of the dust dynamics. Hence the most interesting dynamical phenomena have usually enough time to evolve [5].

Let us dwell upon these features of complex plasmas in detail.

Figure 5 represents different "phase states" of complex plasmas as functions of the electrostatic coupling parameter Γ_{ES} and the mean grain separation Δ, normalized either to the grain size a or to the screening length λ ("finiteness parameter" $\alpha = \Delta/a$ and "lattice parameter" $\kappa = \Delta/\lambda$, respectively). The parameter $\Gamma_{ES} = \Gamma \exp(-\kappa)$, which characterizes the "actual" coupling ratio (potential energy/kinetic energy) at the average intergrain distance, is expressed in terms of the (Coulomb) coupling scale $\Gamma = e^2 Z^2/\Delta T_d$ (note that in terms of Γ and κ, the thermal scattering parameter is $\beta_T^{dd} = 2\Gamma\kappa$). The use of Γ_{ES} implies that the calculations should be representative to some extent of other types of "similar" interaction potentials, too (viz., with "similar" long- and short-range asymptotes). The vertical line $\kappa = 1$ conditionally divides the diagram into weakly screened (Coulomb) and strongly screened (Yukawa) parts. In Fig. 5, we have set $\lambda/a \equiv \alpha/\kappa = 100$, which is typical of complex plasmas studied so far, but there is in principle a wide range of variation, depending on grain size and plasma conditions chosen.

Crystallization in complex plasmas and formation of different lattice types is a widely observed process

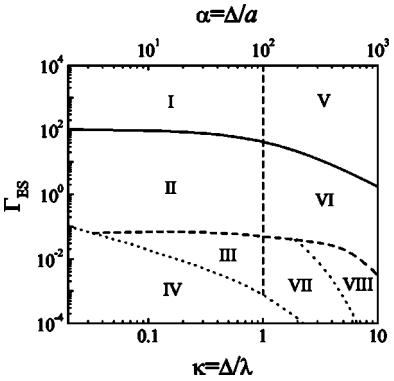

FIG. 5. Phase diagram of complex plasmas in (Γ_{ES},κ) parameter space. The vertical dashed line at $\kappa=1$ conditionally divides the system into "Coulomb" and "Yukawa" parts. Different states are marked in the figure. Regions I (V) represent Coulomb (Yukawa) crystals; regions II (VI) are for Coulomb (Yukawa) nonideal plasmas; regions III (VII and VIII) correspond to Coulomb (Yukawa) ideal plasmas; note that in the region VIII, the pair Yukawa interaction asymptotically reduces to the hard sphere limit, forming a "Yukawa granular medium"; in region IV, the electrostatic interaction is not important and the system is like a usual granular medium. For further explanations, see text.

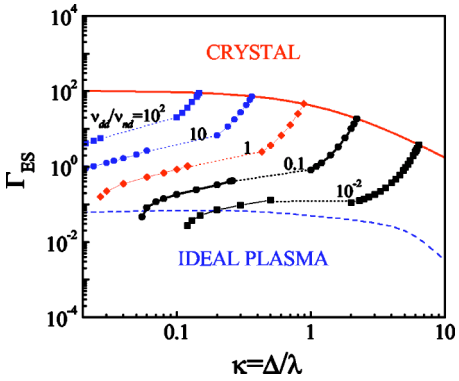

FIG. 6. Typical contours are shown of constant ratios of the momentum transfer rates in grain-grain collisions relative to grain-background (neutral gas) collisions. The values $\nu_{dd}/\nu_{nd}=10^2,10,1,10^{-1}$, and 10^{-2} are depicted in a phase diagram for complex plasmas in (Γ_{ES},κ) parameter space. The parameters used in the calculation are given in the text. Also shown in the figure are the lines corresponding to crystal melting (solid line) and the boundary between ideal and nonideal plasmas (dashed line).

[32–35,38–40]. From the phenomenological point of view, the condition for crystallization is basically determined by the well-known Lindemann criterion [41,42]. The resulting melting line $\Gamma_{ES}^{M}(\kappa)\simeq 106\left(1+\kappa+\frac{1}{2}\kappa^2\right)^{-1}$ is shown in Fig. 5 by the upper solid line.

Further insight into the possible phase states shown in Fig. 5 is obtained from our above results for the momentum transfer cross section for grain-grain collisions. This approach allows us to obtain a clear physical classification of complex plasmas. The dashed line indicates the "transition" between "ideal" and "nonideal" plasmas. We determine this transition from the condition $\sqrt{\sigma/\pi}=(4\pi/3)^{-1/3}\Delta$, which implies that the characteristic range of grain interaction (in terms of the momentum transfer) is comparable to the intergrain distance (in terms of the Wigner-Seitz radius). Above this line, the interaction is essentially multiparticle, whereas below the line only pair collisions are important. This refines the standard condition used to define a "boundary" between ideal and nonideal plasmas, $\Gamma_{ES}\sim 1$. From the thermodynamical point of view, this line determines the limit of employing expansions of the thermodynamical functions (e.g., virial expansion) over the (small) coupling parameter. It is important to note that for a Yukawa potential (as well as for any monotonic interaction potential), thermodynamics predicts that there is no liquid-gas phase transition (i.e., the critical point occurs at $T_d=0$ for such systems). This is different if the pair potential is not monotonic, e.g., a long-range attractive component added to a repulsive electrostatic potential exists, as has been suggested by some authors (see, e.g., Refs. [1,6,10]). So far, however, there are no reliable experiments reporting on the observation of, e.g., the coexistence of liquid and gaseous phases, or other indications of a first-order phase transition in gaseous complex plasmas.

The regions where the system is similar to a granular medium are also shown in Fig. 5: Below the lower dotted curve the electrostatic interaction is too weak and the momentum exchange occurs due to direct grain collisions, i.e., we have a usual granular medium where charges do not play any noticeable role. This line corresponds to $\beta_T^{dd}=(a/\lambda)\Lambda_{dd}^{-1/2}$ [see Eq. (11)].

The upper dotted curve marks the transition boundary for a very interesting state, which we have called the "Yukawa granular medium." Here the "mean" scattering parameter for grain-grain collisions exceeds unity $(\beta_T^{dd}>1)$ and, hence, the strongly screened electrostatic interaction reduces asymptotically to the hard-sphere limit with radius $R_0\simeq\lambda\ln(2\beta_T^{dd})$.

Next we investigate complex plasma properties in terms of the competition between the momentum transfer in mutual grain-grain collisions and the interaction with the surrounding medium.

Complex plasmas can be "engineered" as essentially a "one-phase fluid" (when the interactions between the grains dominate), or as a "particle laden two-phase flow" (when the interactions with the background medium are of similar or greater importance). We have illustrated this by plotting contours of constant ratios of the grain-grain/grain-background momentum transfer rates, ν_{dd}/ν_{nd}, in the (Γ_{ES},κ) diagram in Fig. 6. The characteristic momentum-transfer rate in grain-grain collisions is given either by Eq. (21) or Eq. (23). In complex plasmas, the exchange of momentum with the background medium is mostly through grain-neutral gas collisions,

$$\nu_{nd}=\delta(8\sqrt{2\pi}/3)(m_n/m_d)a^2n_nv_{T_n},$$

where m_n, n_n, and v_{T_n} are the mass, density, and thermal velocity of neutrals, respectively [43]. The value of the numerical factor $\delta=1+\pi/8\simeq 1.4$, corresponding to diffuse scattering with full accommodation, is chosen in accordance with recent experimental results [44]. For the calculations we use the following parameters: Grains of radius $a=1$ μm and material mass density of 1 g/cm^3 in argon plasma at neutral

gas pressure 100 Pa, room-temperature ions and neutrals $T_i \sim T_n \sim 0.03$ eV, and $a/\lambda = 10^{-2}$. For the momentum-transfer rate, we use Eq. (23) at $\beta_T^{dd} \gg 1$ (upper symbols in the figure) and Eq. (21) at $\beta_T^{dd} \ll 1$ (lower symbols). In the transition regime $\beta_T^{dd} \sim 1$, none of these approximations is applicable and we have therefore simply linked the two regimes by dotted lines.

Figure 6 shows that there is a broad range of parameters where complex plasmas have the properties of one-phase fluids ($\nu_{dd}/\nu_{nd} \gg 1$) and those of two-phase fluids $\nu_{dd}/\nu_{nd} \sim 1$. In the extreme limit of very small ν_{dd}/ν_{nd}, we can also, of course, have "tracer particles" in the background medium, which provide practically no disturbance to the background flow. Taking into account that a number of plasma parameters (e.g., the neutral gas pressure, plasma screening length, and the ratio a/λ) can be varied relatively easily within approximately one order of magnitude, most of the possible states can be investigated.

V. DISCUSSION AND CONCLUSIONS

There are a number of reasons why complex plasmas are of great importance for fundamental physics. For instance, one can study the kinetics of crystallization and melting in real time. The nucleation and the subsequent growth of crystalline structures in complex plasmas look very similar to usual crystallization experiments (e.g., in semiconductors). It is reasonable, therefore, to conclude that space- and time-resolved investigation of elementary processes accompanying the nucleation and growth of plasma crystals can be very useful for understanding some basic microscopic processes in liquid-solid phase transitions. Plasma crystals give us an excellent opportunity to study wave phenomena relevant to transport in usual crystals (e.g., thermal conductivity)—nonlinear mode interaction, umklapp processes, phonon scattering on defects, etc. at the kinetic level. Also, complex plasmas are particularly suitable for kinetic investigations of elementary processes in fluids [45]. This suggests that we apparently have a powerful new tool for investigating fluid flows on (effectively) nanoscales, including the all-important transition from collective fluid behavior to individual kinetic behavior, as well as nonlinear processes on scales that have not been accessible for studies so far.

In this paper, we investigated various modes of momentum transfer in complex plasmas using a screened Coulomb potential for the dust grains: electron-grain, ion-grain, and grain-grain collisions. Electron-grain and ion-grain collisions give rise to the so-called electron and ion drag forces, which can influence (or even determine) grain transport in plasmas. The consideration of momentum transfer in grain-grain collisions allowed us to obtain a clear physical classification of the possible complex plasma states. We showed that different "phases" are possible, including crystalline, ideal, and non-ideal plasmas, and two types of granular media. The boundaries between these states were defined and summarized in a (sample) phase diagram. We also showed that complex plasmas can exist in a broad range of dynamical states (one- and two-phase fluids, as well as tracer particles). This broad range of states that is accessible for complex plasmas and the possibility to study a variety of processes at the kinetic level make these systems extremely attractive for further research.

[1] V. N. Tsytovich, Usp. Fiz. Nauk **167**, 57 (1997) [Phys. Usp. **40**, 53 (1997)].
[2] G. E. Morfill, H. M. Thomas, U. Konopka, and M. Zuzic, Phys. Plasmas **6**, 1769 (1999).
[3] A. Piel and A. Melzer, Plasma Phys. Controlled Fusion **44**, R1 (2002).
[4] S. V. Vladimirov and K. Ostrikov, Phys. Rep. **393**, 175 (2004).
[5] G. E. Morfill *et al.*, Phys. Scr., T **107**, 59 (2004).
[6] V. E. Fortov, A. G. Khrapak, S. A. Khrapak, V. I. Molotkov, and O. F. Petrov, Usp. Fiz. Nauk **174**, 495 (2004) [Phys. Usp. **47**, 447 (2004)].
[7] V. N. Tsytovich, G. E. Morfill, and H. Thomas, Plasma Phys. Rep. **28**, 623 (2002).
[8] G. E. Morfill, V. N. Tsytovich, and H. Thomas, Plasma Phys. Rep. **29**, 1 (2003).
[9] H. Thomas, G. E. Morfill, and V. N. Tsytovich, Plasma Phys. Rep. **29**, 895 (2003).
[10] S. A. Khrapak, A. V. Ivlev, and G. Morfill, Phys. Rev. E **64**, 046403 (2001).
[11] A. V. Ivlev *et al.*, Phys. Rev. Lett. **92**, 205007 (2004).
[12] L. D. Landau and E. M. Lifshitz, *Mechanics* (Pergamon, Oxford, 1960).
[13] S. A. Khrapak, A. V. Ivlev, G. E. Morfill, and H. M. Thomas, Phys. Rev. E **66**, 046414 (2002).
[14] S. A. Khrapak, A. V. Ivlev, G. E. Morfill, and H. M. Thomas, in *Dusty Plasma in the New Millennium*, edited by R. Bharuthram, M. A. Hellberg, P. K. Shukla, and F. Verheest, AIP Conf. Proc. No. 649 (AIP, Melville, NY, 2002), p. 341.
[15] S. A. Khrapak, A. V. Ivlev, G. E. Morfill, and S. K. Zhdanov, Phys. Rev. Lett. **90**, 225002 (2003).
[16] S. A. Khrapak, A. V. Ivlev, G. E. Morfill, S. K. Zhdanov, and H. Thomas, IEEE Trans. Plasma Sci. **32**, 555 (2004).
[17] G. H. Lane and E. Everhart, Phys. Rev. **117**, 920 (1960).
[18] B. M. Smirnov, Sov. Phys. Usp. **25**, 854 (1982).
[19] E. M. Baroody, Phys. Fluids **5**, 925 (1962).
[20] H.-S. Hahn, E. A. Mason, and F. J. Smith, Phys. Fluids **14**, 278 (1971).
[21] M. D. Kilgore, J. E. Daugherty, R. K. Porteous, and D. B. Graves, J. Appl. Phys. **73**, 7195 (1993).
[22] J. Allen, Phys. Scr. **45**, 497 (1992).
[23] R. V. Kennedy and J. E. Allen, J. Plasma Phys. **69**, 485 (2003).
[24] J. E. Allen, B. M. Annaratone, and U. de Angelis, J. Plasma Phys. **63**, 299 (2000).
[25] A. V. Zobnin *et al.*, JETP **91**, 483 (2000).
[26] M. Lampe *et al.*, Phys. Plasmas **10**, 1500 (2003).
[27] S. Ratynskaia *et al.*, Phys. Rev. Lett. **93**, 085001 (2004).
[28] S. A. Khrapak and G. E. Morfill, Phys. Rev. E **69**, 066411

(2004).
[29] S. Benkadda, P. Gabbai, V. N. Tsytovich, and A. Verga, Phys. Rev. E **53**, 2717 (1996).
[30] G. E. Morfill *et al.*, Plasma Phys. Controlled Fusion **44**, B263 (2002).
[31] D. H. E. Dubin and T. M. O'Neil, Rev. Mod. Phys. **71**, 87 (1999).
[32] J. H. Chu and Lin I, Phys. Rev. Lett. **72**, 4009 (1994).
[33] H. Thomas *et al.*, Phys. Rev. Lett. **73**, 652 (1994).
[34] Y. Hayashi, Phys. Rev. Lett. **83**, 4764 (1999).
[35] A. Melzer, A. Trottenberg, and A. Piel, Phys. Lett. A **191**, 301 (1994).
[36] A. M. Lipaev *et al.*, JETP **85**, 1110 (1997).
[37] S. Khrapak *et al.*, Phys. Plasmas **10**, 1 (2003).
[38] H. M. Thomas and G. E. Morfill, Nature (London) **379**, 806 (1996).
[39] M. Zuzic *et al.*, Phys. Rev. Lett. **85**, 4064 (2000).
[40] A. P. Nefedov *et al.*, New J. Phys. **5**, 33.1 (2003).
[41] O. S. Vaulina and S. A. Khrapak, JETP **90**, 287 (2000).
[42] O. Vaulina, S. Khrapak, and G. Morfill, Phys. Rev. E **66**, 016404 (2002).
[43] P. S. Epstein, Phys. Rev. **23**, 710 (1921).
[44] B. Liu *et al.*, Phys. Plasmas **10**, 9 (2003).
[45] G. E. Morfill *et al.*, Phys. Rev. Lett. **92**, 175004 (2004).